

DEPENDENCE OF OPTICAL ACTIVE GALACTIC NUCLEI IDENTIFICATION  
ON STELLAR POPULATION MODELS

YAN-PING CHEN,<sup>1</sup> INGYIN ZAW,<sup>1,2</sup> AND GLENNYS R FARRAR<sup>2</sup>

<sup>1</sup>*New York University Abu Dhabi, P.O. Box 129188,  
Abu Dhabi, United Arab Emirates*

<sup>2</sup>*Center for Cosmology and Particle Physics,  
Physics Department, New York University,  
New York, NY 10003, USA.*

Submitted to ApJ

ABSTRACT

We have conducted a study to quantify the systematic differences resulting from using different stellar population models in optical spectroscopic identification of type II AGN. We examined the different AGN detection fractions of 7069 nearby galaxies ( $z \leq 0.09$ ) with SDSS DR8 spectra when using the [Bruzual & Charlot \(2003, BC03\)](#), [Vazdekis et al. \(2010, MILES\)](#), and solar metallicity [Maraston and Strömbäck \(2011\)](#) (MS11<sub>solar</sub>) stellar population models. The line fluxes obtained using BC03 and MS11<sub>solar</sub> are publicly available from SDSS data releases. We find that the BC03 templates result in systematically higher BPT line ratios and consequently higher AGN fractions and the MS11<sub>solar</sub> templates result in systematically lower line ratios and AGN fractions compared with the MILES templates. Using MILES as the standard, BC03 results in 25% “false positives” and MS11<sub>solar</sub> results in 22% “false negatives” when using the [Kewley et al. \(2001a\)](#) boundary for AGN identification. The fraction of galaxies whose AGN identification changes for different templates is luminosity dependent, ranging from a few percent for  $L_{[OIII]5007} \geq 10^{40}$  erg  $s^{-1}$  and increasing to  $\sim 50\%$  for  $L_{[OIII]5007} \leq 10^{38}$  erg  $s^{-1}$ . These results suggest that template choice should be accounted for when using and comparing the AGN and emission line fluxes from different catalogs.

*Keywords:* galaxies: active – galaxies: nuclei – techniques: spectroscopic

## 1. INTRODUCTION

Optical spectroscopy is a powerful tool to probe the physical properties of active galactic nuclei (AGN). Broad-line (type I) AGN are characterised by their broad hydrogen Balmer lines, with Full Width at Half Maximum (FWHM) values up to a few thousand  $\text{km s}^{-1}$ . Narrow-line (type II) AGN however, need to be distinguished from star-forming galaxies since they emit the same set of ionised forbidden lines such as [N II] 6584 and [O III]5007. The differences in the ratios of these lines to the narrow hydrogen Balmer lines (i.e.,  $H\alpha$ , and  $H\beta$ ) between AGN and star-forming galaxies were first reported by Baldwin, Phillips and Terlevich (1981, hereafter, BPT), and further explored by others (e.g., Osterbrock & Pogge 1985; Veilleux & Osterbrock 1987; Kewley et al. 2001a; Kauffmann et al. 2003; Stasińska et al. 2006; Kewley et al. 2006; Cid Fernandes et al. 2010, 2011). Kewley et al. (2001a) developed separation criteria based on theoretical modeling of star formation lines, while Kauffmann et al. (2003) defined empirical separation criteria based on Sloan Digital sky Survey (SDSS, York et al. 2000) spectra.

The spectra of galaxies containing AGN show not only emission features but also stellar absorption lines and continuum emission from the host galaxies. Subtraction of the host galaxy contribution to the integrated light in previous works (e.g., Ho et al. 1997; Kewley et al. 2000, 2001b; Kauffmann et al. 2003) has been done either with a local polynomial fit or using templates (e.g., Bruzual & Charlot 2003). The former is easy to perform, does not rely on any models, and can be straightforwardly applied as a quick solution for the absorption and continuum components estimation, especially for objects with very strong emission features (e.g., those of Seyfert I AGN). However, when the spectrum contains non-negligible absorption features, the accuracy of the emission line fluxes can be affected. Weak emission line features, especially hidden in the absorption and continuum components, can easily be underestimated in a local polynomial continuum fit. In these cases, using stellar templates to fit the absorption and continuum gives a more accurate solution. Full-spectrum-fitting and subtraction of absorption and continuum components requires strong enough absorption features to match with stellar templates. Instead of full-spectrum-fitting, one can also use principle component analysis (PCA) (e.g., Hao et al. 2005a; Greene & Ho 2007; Allen et al. 2013) to determine the underlying galaxy spectra and to extract the emission lines.

Several studies based on AGN spectroscopic identification have been published (e.g., Kauffmann et al. 2003; Miller et al. 2003; Kewley et al. 2006) using SDSS data. The AGN detection rate is known to depend on the details of data processing (Hao et al. 2005a): redshift ranges, signal-to-noise cut of the data, and the boundary that separates type II AGN from star-forming galaxies in BPT diagrams (i.e., the authors may have different AGN identification criteria).

In this work, we consider the impact of the using different stellar population models on AGN identification, which has not previously been quantified. The AGN identification in SDSS data releases first used Bruzual & Charlot (2003, BC03), and currently Maraston and Strömbäck (2011) at solar metallicity only ( $MS11_{solar}$ ), as templates for stellar component analysis. As more stellar population models become available, systematic studies of AGN identification's dependence on the stellar model used become possible. This is important not only for finding the best template, but also for understanding the merits and limitations of the models. In our study, we compare the results from BC03,  $MS11_{solar}$ , and Vazdekis et al. (2010, MILES) stellar population models.

In Section 2, we present both the sample for our study and our procedure for identifying narrow line AGN candidates. In Section 3, we review the stellar population models used in this analysis. We also describe how we applied stellar population models to our data. Our results and the relative effects from varying the templates are presented in Section 4, where we also discuss the aspects of the stellar templates which lead to different results. We present our conclusions in Section 5. The appendix includes other properties we explored that do not cause major differences in type II AGN identification, namely, wavelength range, young stellar populations, Seyfert II vs. LINERs, and data quality.

## 2. DATA SAMPLE AND AGN IDENTIFICATION

This work is part of our efforts to construct an all-sky optical AGN catalog (Zaw, Chen and Farrar, in prep, ZCF18 below), based on optical spectra from the 2MASS Redshift Survey (2MRS, Huchra et al. 2012). The 2MRS was assembled from observations by the 2MRS team (with the FAst Spectrograph for the Tillinghast telescope at the Fred L. Whipple Observatory in the north and Cerro Tololo Interamerican Observatory in the south) and from other catalogs, including the SDSS data release (DR) 8, the 6dF Galaxy Survey, and the NASA Extragalactic Database. Among all the subsamples, the SDSS subsample has the best signal to noise ratios, and the only one where absolute flux calibration and telluric correction has been applied to the spectra. In addition, the line fluxes from SDSS data releases can be used to cross check our work. We therefore use the SDSS subsample for our study. The SDSS subsample

consists of the spectra of 7069 galaxies with a redshift of  $z \leq 0.09$ . These spectra cover the wavelength range 3800–9200 Å, with a mean resolution of  $R \sim 1800$ –2000.

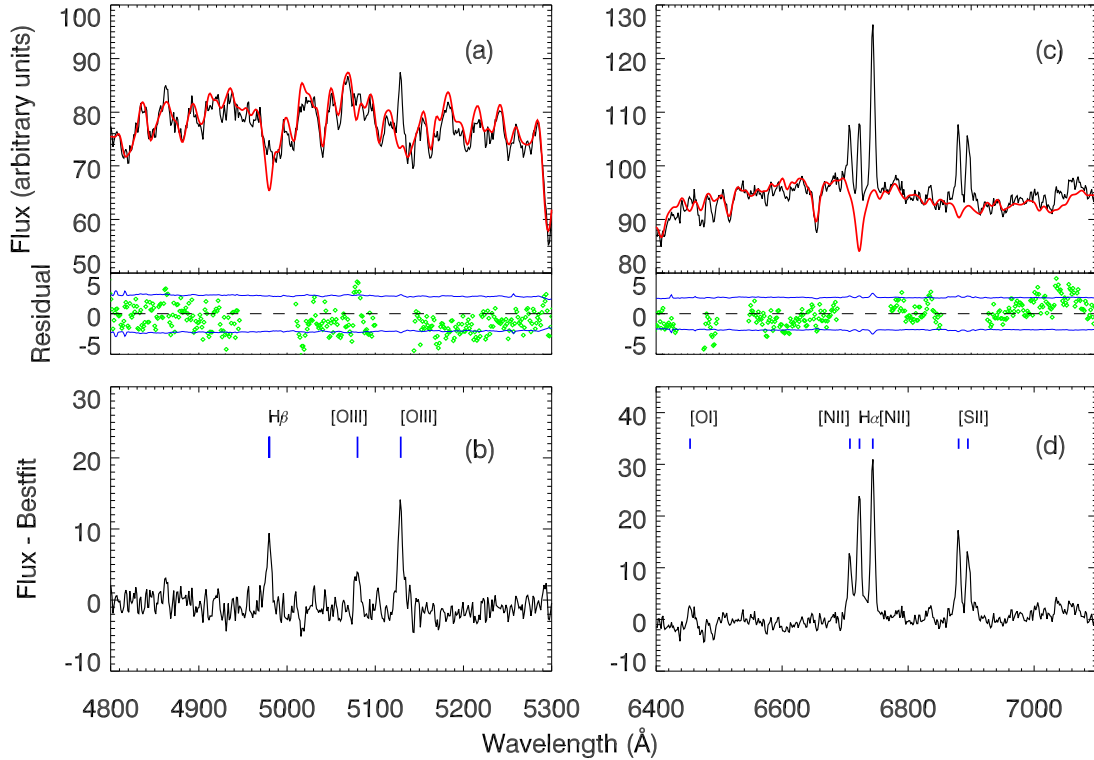


**Figure 1.** An example to illustrate that template subtraction is necessary to identify weak emission lines. Top panels: data are marked as black lines, the best fit models are marked as red lines, the horizontal blue lines are showing the  $1\sigma$  error spectra, the green dots are the residuals in regions without emission lines. Weak  $H\beta$  emission line is absent before template subtraction. Bottom panels: Residual spectra showing the emission line features after subtracting the best-fit (absorption) models.

### 2.1. Type II AGN candidate identification

A detailed description of the emission line galaxy selection is given in our catalog paper (ZCF18). We briefly summarise the process here. After rebinning the data and model spectra to the same spectral resolution, and masking out the AGN identification emission line regions, a full-spectrum-fitting was performed on each SDSS object using pPXF (Cappellari & Emsellem 2004). In the fitting procedure, the model spectra are shifted to the redshift of the observed spectra and broadened to account for stellar velocity dispersion. Each fit consists of a linear combination of model spectra. The fits are required to yield a physical stellar velocity dispersion,  $\sigma_{\text{fit}} < 1000 \text{ km s}^{-1}$ , in order to be considered acceptable. The fitting routine uses the error spectrum, provided with the data, to calculate a reduced  $\chi^2$  value for each acceptable fit. The “best-fit” spectrum is the one which minimizes the reduced  $\chi^2$ . We limit the sample to those spectra whose reduced  $\chi^2$  are less than 2.55 in the full-spectrum-fitting process, which keeps 99% of the spectra with successful fits.

The residual spectrum produced by subtracting the best-fit model from the data spectrum, is used to analyze the emission line features. The galaxies with weak emission lines are most affected by the choice of stellar templates. Figure 1 shows an example where the  $H\beta$  emission line is invisible in the spectrum by eye, but is identified by the template subtraction using MILES (Vazdekis et al. 2010) templates.

In this work, we use  $H\alpha$ ,  $H\beta$ ,  $[\text{O III}] 5007$ , and  $[\text{N II}] 6584$  to identify galaxies as type II AGN. We infer the flux for each of the emission lines from the residual spectrum, by fitting Gaussian profiles. The line fluxes are calculated under the fitted Gaussian profiles within  $3\sigma$  of the line peak, where  $\sigma$  is the fitted Gaussian width of the line. The flux errors (i.e. line noises) are calculated as the sum in quadrature of the error spectra under the same wavelength range of the

emission lines. An emission line is defined as one where the line flux divided by the flux error is greater than three (i.e.  $S/N \geq 3$ ) when using MILES templates. We define emission line galaxies as those where all four diagnostic lines ( $H\beta$ , [O III] 5007,  $H\alpha$  and [N II] 6584) have  $S/N \geq 3$ . There are 3350 emission line galaxies in our sample. We use the BPT line ratios [N II]/ $H\alpha$  and [O III]/ $H\beta$  and the Kewley et al. (2001a) criteria to separate star-forming galaxies and type II AGN candidates, i.e., those above Kewley et al. (2001a) line are taken as type II AGN, those below Kewley et al. (2001a) line are taken as star-forming galaxies.

### 3. MODEL TEMPLATES

Stellar population models (SPM) are constructed by integrating a group of stellar spectra, known as a stellar library, with weights given by the initial mass functions. The group of stars are assumed to share the same age and chemical components, (i.e., metallicity), but with a variety of stellar masses. Their integrated light forms a single stellar population spectrum. The connection between stellar population models and individual stellar spectra are stellar parameters such as effective temperature  $T_{\text{eff}}$ , surface gravity  $\log g$ , and metallicity [Fe/H]. When the stellar populations are constructed, an interpolator is applied to generate the grid of stars used to integrate the light of the population; see Conroy (2013), Vazdekis et al. (2010) and references therein for details. The interpolator is based on the parameter space coverage of the underlying stellar library. When stars are limited to a certain part of the parameter space, the interpolator may be biased if the available data does not adequately span the parameter space. Each stellar population model consists of a set of single stellar population (SSP) templates with a given age and metallicity.

The Bruzual & Charlot (2003) templates are widely used to subtract the stellar absorption components and the continuum, in analyses of emission line galaxies, because they cover a large spectral wavelength range and were developed earlier. In the last decade, with improvements in both data and theoretical modelling, more stellar libraries have been constructed and published (e.g., Chen et al. 2014; Sánchez-Blázquez et al. 2006; Gregg et al. 2006; Prugniel & Soubiran 2001), and their corresponding stellar population models are available (e.g., Vazdekis et al. 2010; Le Borgne et al. 2004; Vazdekis et al. 2016; Maraston and Strömbäck 2011).

In this work we compare the stellar population models of MILES, MS11<sub>solar</sub> MILES-based models, González Delgado et al. (2005, hereafter G05) and BC03. The SDSS fluxes for DR8 were based on host galaxy subtraction using BC03. More recently, Thomas et al. (2013) made public new fluxes for DR8 spectra using MS11<sub>solar</sub>. MILES model is based on observed stellar optical spectra (Sánchez-Blázquez et al. 2006); the BC03 model was constructed from a combination of theoretical and observed spectra. The MS11<sub>solar</sub> MILES based model shares the same input stellar library as MILES model. The G05 model was constructed from theoretical stellar spectra, and is the best available theoretical model. We use them when empirical data are incomplete, e.g., for young stellar populations. The model ingredients are described in section 3.1. Since the MILES models are built from the MILES stellar library, currently the best empirical optical stellar library and widely used by several stellar population models (e.g., Conroy & Gunn (2010); Maraston and Strömbäck (2011); Vazdekis et al. (2010, 2012)), we therefore use the MILES templates as our standard.

#### 3.1. Differences of stellar population models

Stellar population models have several distinct properties. The parameter ranges for the models we compare in this work are given in Table 1. They vary in age and metallicity ranges, as well as in stellar libraries. We will investigate how each of these affects our results. The key ingredients of stellar population models that describe the individual spectra of stellar systems from different sources are as follows. BC03 mainly uses a combination of the empirical stellar library STELIB (Le Borgne et al. 2003) and a series of theoretical stellar libraries BaSeL (Lejeune, Cuisinier, & Buser 1997, 1998; Westera et al. 2002). The BC03 SSPs are likely to be biased in the optical, having been built from the STELIB library that contains 249 stars, with very few stars at non-solar metallicities. The MILES model is based on the empirical MILES stellar library that covers a wide range of stellar parameter space (i.e.,  $T_{\text{eff}}$ ,  $\log g$ , and [Fe/H]), with four times more stars than in STELIB. The G05 model is based on a theoretical stellar library; they contain a wide age range, helpful in understanding the contribution from younger stellar components in the host galaxies. The MILES-based MS11 model used the same stellar library as MILES, with a special procedure for integrating the light of thermally pulsing asymptotic giant branch (TP-AGB) stars. The MS11<sub>solar</sub> templates are the subset of MILES-based MS11 SPM that assume solar metallicity abundances.

We also note that the resolutions of different SPMs are different, but this does not have a significant impact on our results, since the SDSS spectra have lower or similar resolution as the template libraries. In addition, the velocity dispersions in host galaxies (a few hundred  $\text{km s}^{-1}$ ) are bigger than the differences in resolution (a few tens  $\text{km s}^{-1}$ )

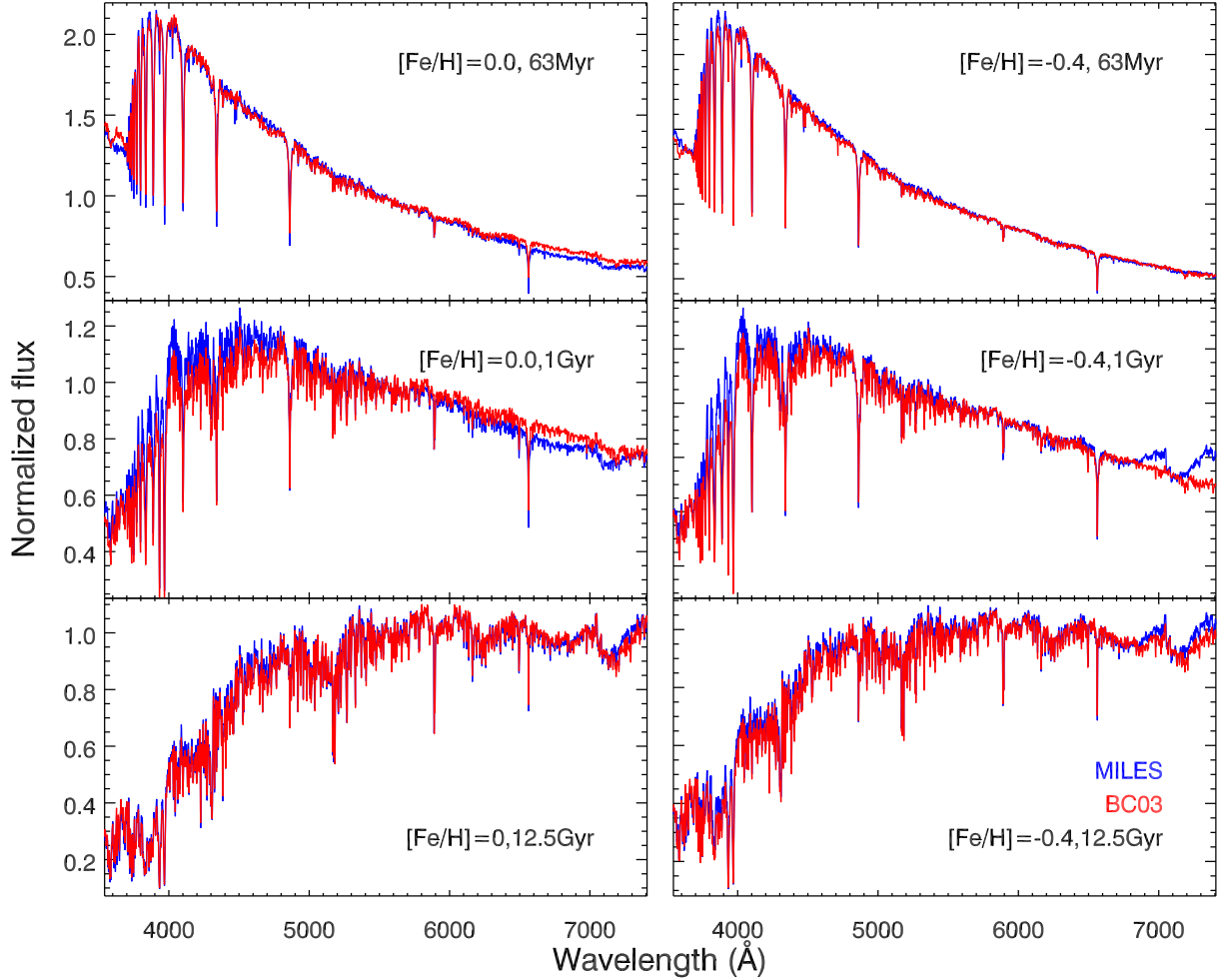


**Figure 2.** Full spectrum model comparison, spectra were normalised at  $\lambda\lambda$  5500Å. MILES templates were smoothed to the same resolution as BC03 for fair comparison. Note the discrepancies at long wavelength, and the systematically lower flux of BC03 in the 4000–5000 Å range in the middle panels.

**Table 1.** Stellar population models used for this work and their properties.

Source	Wavelength range	Resolution	Age range	Metallicity (Z) range
BC03	91Å-160 $\mu$ m	3Å	0.1Myr-20Gyr	Z=0.004 – 0.05
MILES ssp	3500-7500Å	2.51Å	0.06-15Gyr	Z=0.0001 – 0.03
G05	3000-7000Å	0.3Å	4Myr-17Gyr	Z=0.004 – 0.019
MS11 <sub>solar</sub>	3500 - 7429Å	2.54Å	6.5 Myr-15 Gyr	Z=0.02 (solar metallicity)

Notes: The [Bruzual & Charlot \(2003\)](#) model has a resolution of 3Å from 3200–9500Å, and lower resolution in other wavelength ranges. G05 refers to the model published in [González Delgado et al. \(2005\)](#). We used the Padova isochrone choice for the MILES and G05 models. We used the MILES based stellar population from MS11 at solar metallicity only in this work to compare with [Thomas et al. \(2013\)](#).

of the stellar population models whose resolution is determined by the stellar libraries used. When comparing the models with the observations, broadening the stellar models to fit the spectral features of the observations erases the resolution differences. Therefore, the resolution difference issue is not further discussed in this work.

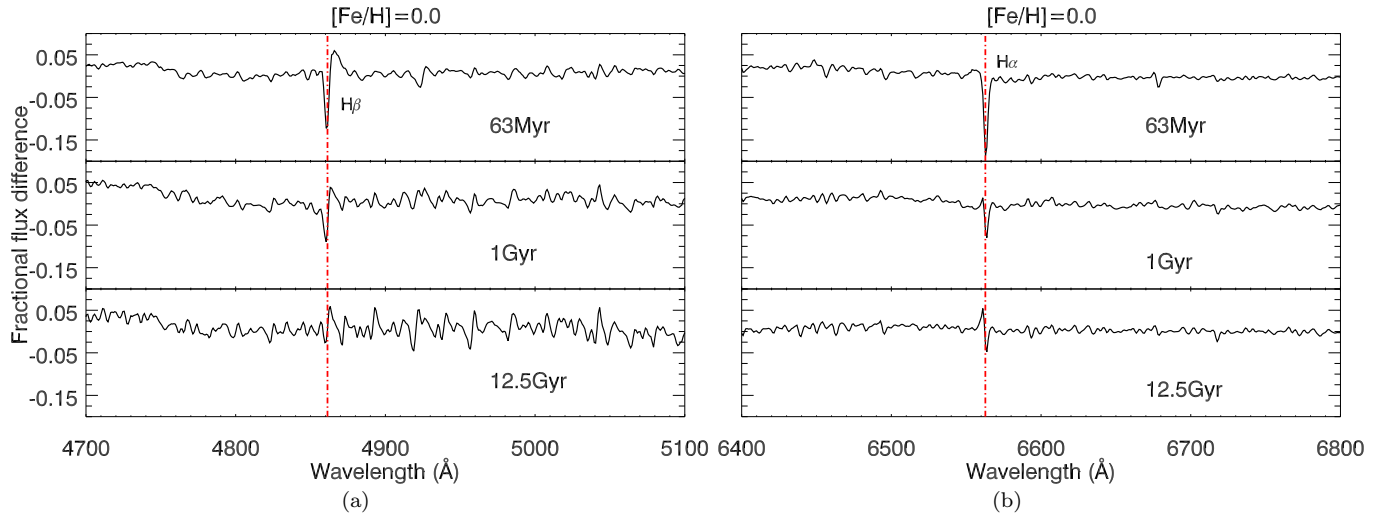


**Figure 3.** Left: Model comparison zoomed in the blue at solar metallicity ( $[\text{Fe}/\text{H}] = 0.0$ ), spectra were normalised at  $\lambda\lambda$  4830Å. Right: Model comparison zoomed in the red at same metallicity, spectra were normalised at  $\lambda\lambda$  6520Å. The fractional flux difference is derived by taking the difference between MILES models and BC03, normalized to MILES models.

### 3.2. Spectral line features of stellar population models

We first directly compare different stellar population templates from each SPM available with the same parameters (i.e., age, metallicity, and initial mass function), as the spectral line features are particularly important in the subtraction procedure to yield the type II AGN candidates. In Figure 2 we show the MILES and BC03 stellar population templates for representative ages of 63 Myr, 1 Gyr and 12.5 Gyr at solar ( $[\text{Fe}/\text{H}] = 0.0$ ) and sub-solar metallicity ( $[\text{Fe}/\text{H}] = -0.4$ ). We see that for a given population, these two sets of models agree best at older ages (12.5 Gyr) with solar metallicity. At younger ages, i.e., 63 Myr and 1 Gyr, inconsistencies are seen in both the Balmer lines and the overall shapes (i.e., the colors). At sub-solar metallicity, there are inconsistencies in the red,  $\sim 6800\text{--}7400$  Å, especially for older populations. Although we have normalised the models at  $5500\text{Å}$ , there are still some color discrepancies.

To better understand the similarities and differences of the models in the wavelength ranges of the four main type II AGN identification lines, we zoom in on the SSPs. In Fig 3a, we see that at solar metallicity, these two sets of models agree with each other especially at older ages (12.5 Gyr). However, models show differences in the depth of  $\text{H}\alpha$  (Fig 3b) at younger ages, with a 7% of difference observed for 1 Gyr models. In general, MILES templates show stronger absorption Balmer lines than BC03.

We show the MILES-based  $\text{MS11}_{\text{solar}}$  and compare them with MILES SSPs in Figs 4a and 4b. Although both  $\text{MS11}_{\text{solar}}$  and MILES used the MILES stellar library as their optical input, we still observe remarkable line differences and continuum variation, due to the other inputs that comprise a SPM. The MS11 models tend to have slightly stronger Balmer absorption lines than MILES at the youngest and oldest ages, but have weaker Balmer absorption lines than MILES at intermediate ages (1 Gyr).

## 4. IS TYPE II AGN IDENTIFICATION TEMPLATE-DEPENDENT?

To check our method and the validity of our results, we compared our line fluxes with the values in the SDSS data release for the emission line galaxies identified by our MILES-based template subtraction. Note that we use the MILES stellar population model while SDSS DR8 uses BC03; therefore some differences in emission line fluxes are expected. The comparison between the fluxes of diagnostic lines ( $\text{H}\beta$ ,  $[\text{O III}]$  5007,  $\text{H}\alpha$  and  $[\text{N II}]$  6584) from our fits and those from SDSS shows a good linear correlation (see ZCF18). The  $\text{H}\beta$  line is the weakest in general, so the scatter is larger than in the other lines.

Although the line fluxes correlate well overall, AGN identification based on the line flux ratios  $[\text{O III}]$  5007/ $\text{H}\beta$  and  $[\text{N II}]$  6584/ $\text{H}\alpha$  may have significant differences. Since galaxies near the boundary are the most likely to shift categories (AGN to star-forming galaxies or vice versa), we begin to examine differences in line ratio by selecting a subsample of objects within 0.02 dex of the Kewley et al. (2001a) boundary using MILES stellar population templates for host galaxy subtraction. This subsample contains 145 emission line galaxies.

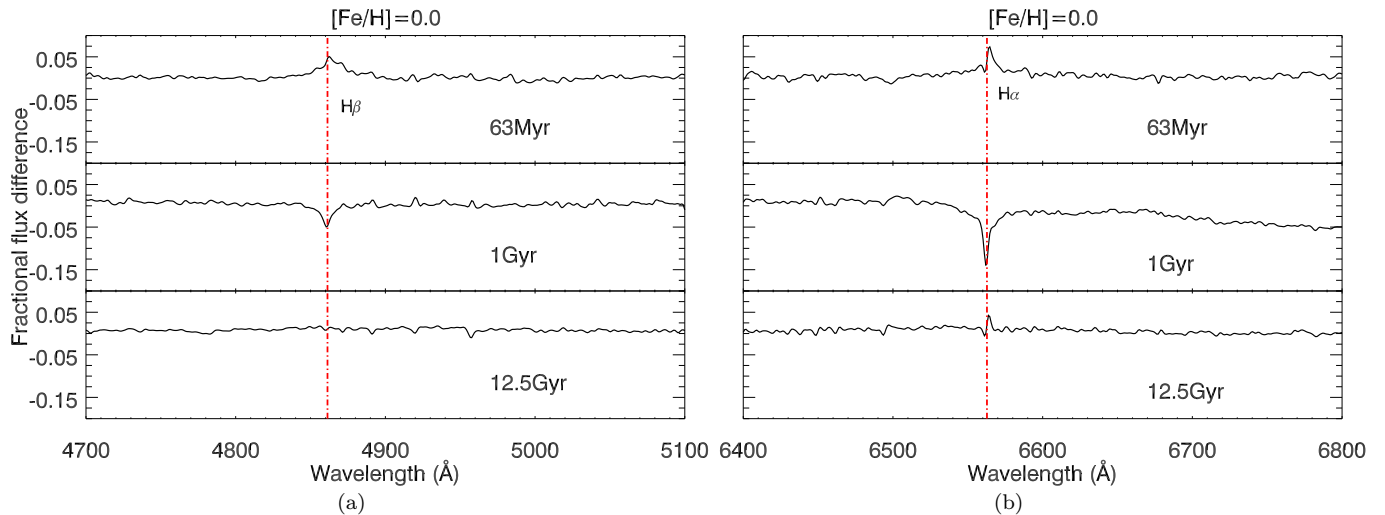


**Figure 4.** Solar metallicity ( $[\text{Fe}/\text{H}] = 0.0$ ) model comparison between MILES and MS11. Both models are smoothed to the same resolution as in BC03. Left: Model comparison zoomed in for blue wavelength ranges. Spectra were normalised at  $\lambda 4830\text{\AA}$ . Right: Model comparison zoomed in for red wavelength ranges. Spectra were normalised at  $\lambda 6520\text{\AA}$ . The fractional flux difference is derived by taking the difference between MILES models and MS11, normalized to MILES models.

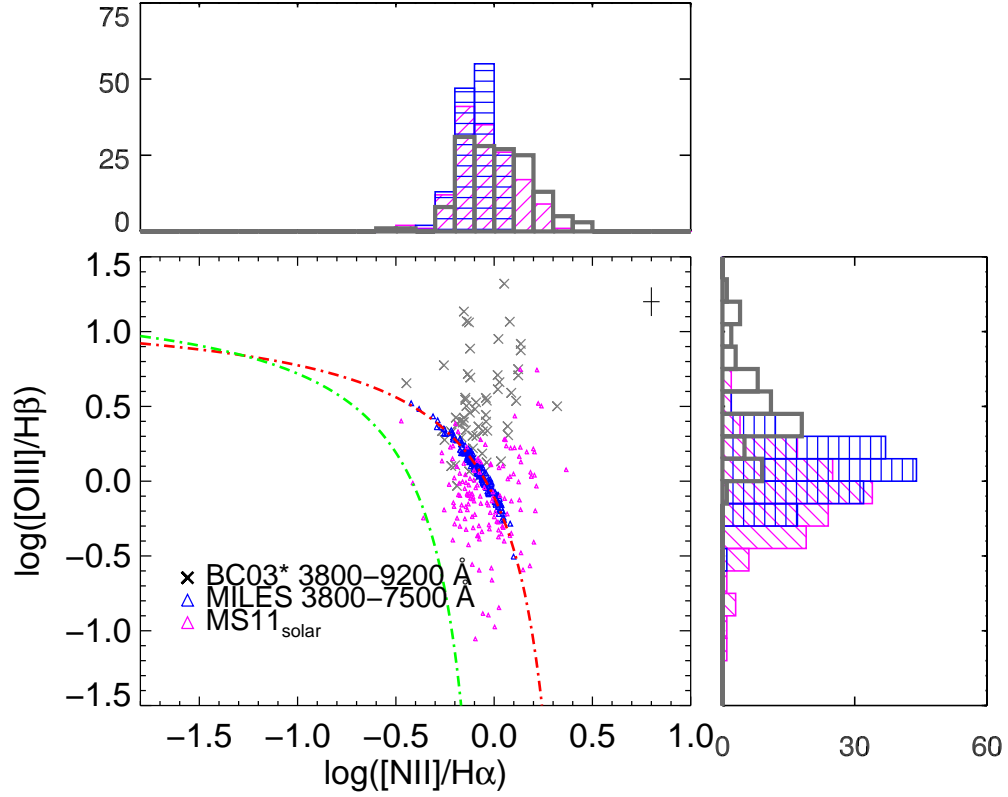
#### 4.1. Type II AGN identification variations

Fig 5 shows the BPT diagram for this boundary sample, with MILES-based line ratios marked as blue triangles, BC03-based line ratios (Aihara et al. 2011) shown as grey crosses, and the MILES-based MS11<sub>solar</sub> (Thomas et al. 2013) result shown as magenta triangles. The line ratios using BC03 are systematically higher than those using MILES. Evidently, more galaxies are classified as AGN when the background galaxy subtraction is processed with BC03 templates, while the line ratios from using MS11<sub>solar</sub> templates are systematically shifted into the composite region, i.e., between Kewley et al. (2001a) and Kauffmann et al. (2003) boundaries. The systematic shift of line ratios from MS11<sub>solar</sub> templates are also seen in the histogram, especially in the line ratio of  $[\text{O III}] 5007/\text{H}\beta$ . BC03 templates result in higher  $[\text{O III}] 5007/\text{H}\beta$  ratios than MILES, while MS11<sub>solar</sub> templates result in lower  $[\text{O III}] 5007/\text{H}\beta$  ratios than MILES. The line ratio of  $[\text{N II}] 6584/\text{H}\alpha$  remains in the similar range.

We then expanded our study to the full emission line sample defined by MILES template subtraction. The BPT diagram for these 3350 galaxies is shown in Fig 6. The narrow emission line galaxies are shown as grey crosses, type II AGN (MILES based) are shown as blue triangles. In panels (b) and (c), we show the line ratios from fluxes when using BC03 and MS11<sub>solar</sub> templates, respectively, for the same galaxies. The symbols reflect AGN identification based on MILES template subtraction. We see that BC03-based line ratios tend to move toward the AGN region, except for a few outliers. MS11<sub>solar</sub> based line ratios move in the opposite direction, and some of the MILES-based AGN shift into the composite region.

In order to learn which type II AGN are most sensitive to the choice of stellar templates, we examine two classes of misidentification, taking the result from MILES template-subtraction as the standard. The first class is type II AGN identified by BC03 but not identified by MILES templates, i.e., “false positives”; the second class is type II AGN identified by MILES templates but not identified by MS11<sub>solar</sub>, i.e., “false negatives”. Since  $[\text{O III}]$  luminosity is an indicator of the AGN bolometric luminosity, we use it to determine whether the misidentification rate depends on AGN activity. We show the  $[\text{O III}]$  luminosity distribution of BC03 type II AGN in Fig 7a. The clear histogram shows the  $[\text{O III}]$  luminosity of 562 type II AGN identified by using BC03 templates, selected from the MILES emission line galaxy sample; the green histogram shows the false positives. We find that 25% of BC03 type II AGN are false positives<sup>1</sup>. The fainter the object is, the more likely it is to be misidentified as an AGN. We show the ratio of misidentification of type II AGN candidates as a function of  $[\text{O III}]$  luminosity in Fig 7b. The largest misidentification rate,  $\sim 50\%$ , is found for galaxies with  $[\text{O III}]$  luminosity fainter than  $\sim 10^{38} \text{ erg s}^{-1}$ .

<sup>1</sup> False negatives from BC03 and false positives from MS11<sub>solar</sub> are negligible (less than 2%).



**Figure 5.** BC03-based line ratios (grey crosses) for 145 objects which MILES-based ratios (blue triangles) within 0.02 dex of the Kewley et al. (2001a) boundary. The MS11<sub>solar</sub> line ratios for the same galaxies (magenta triangles) systematically shift downwards.

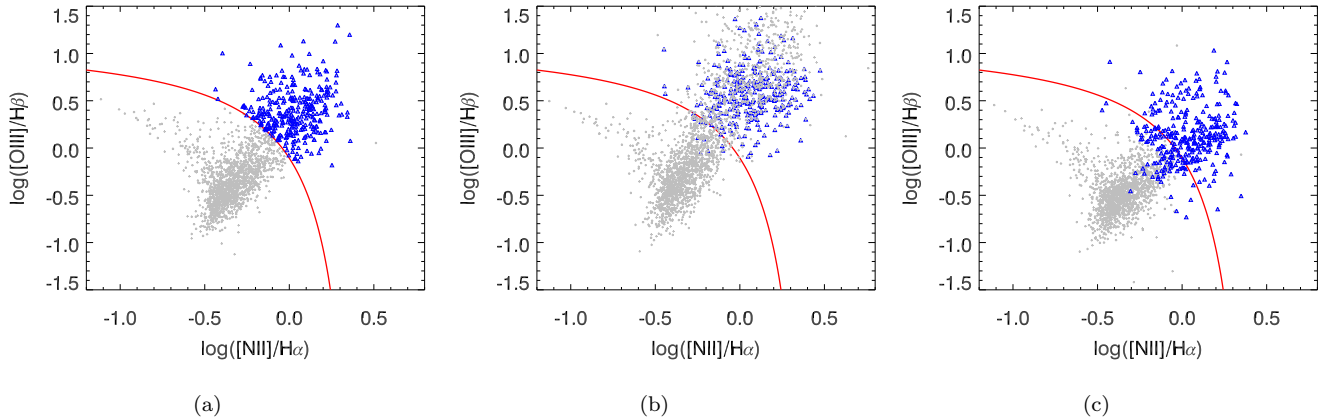


**Figure 6.** Panel (a): Line ratios based on MILES template-subtraction to show the distribution of star-forming galaxies (grey crosses), and AGN (blue triangles). The data are restricted to have  $S/N \geq 3$  for all four lines using the MILES template-subtraction. Panel (b): Line ratios based on BC03 for the same galaxies in panel (a). Panel (c): Line ratios based on MS11<sub>solar</sub> for the same galaxies in panel (a).



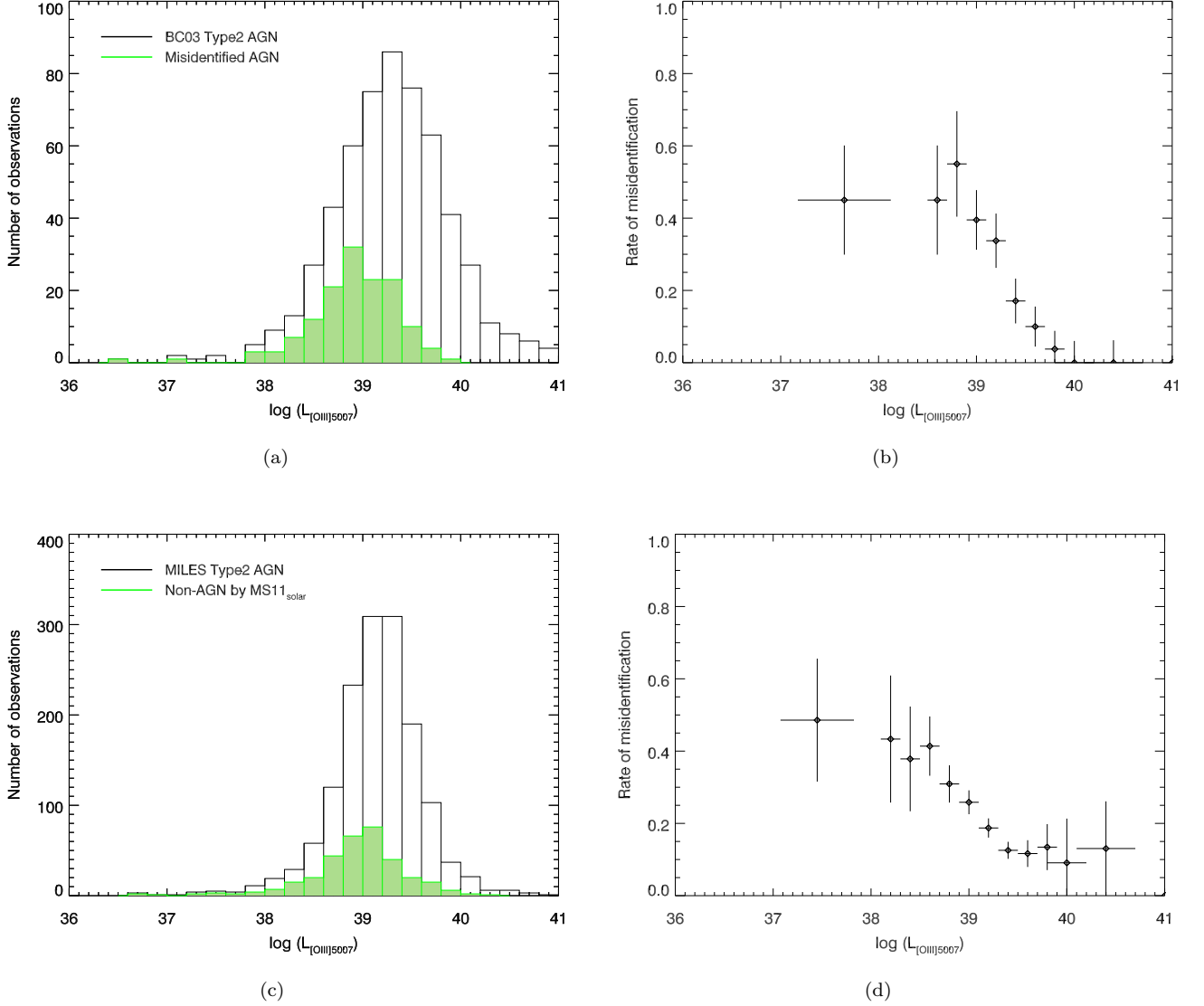


**Figure 7.** Panel (a): The clear histogram shows the [O III]5007 luminosity distribution of type II AGN identified by using BC03 templates. The objects not identified as AGN by using MILES templates are shown in green. Panel (b): Rate of misidentified type II AGN using BC03 templates as a function of [O III]5007 luminosity. Panel (c): The clear histogram shows the [O III]5007 luminosity distribution of type II AGN candidates identified by using MILES templates. The objects not identified as AGN by the work of using MS11<sub>solar</sub> are shown in green. Panel (d): Rate of misidentification of type II AGN by MS11<sub>solar</sub> as a function of [O III]5007 luminosity.

In Fig 7c, type II AGN identified by MILES templates are shown in the clear histogram. Those false negatives when using line ratios from MS11<sub>solar</sub> template subtraction are shown in the green histogram. A total misidentification rate of 22% is observed. We plot the misidentification rate as a function of [O III]5007 luminosity in Fig 7d: objects with [O III]5007 luminosity fainter than  $10^{38}$  erg  $s^{-1}$  can have a misidentification rate as large as  $\sim 50\%$ .

Furthermore, we limit the 2MRS-SDSS sample to have  $S/N \geq 3$  for all four AGN diagnostic lines for all three sets of templates to avoid effects of low signal to noise, which results in 2300 remaining galaxies. As shown in Fig 8, there is still a clear systematic shift between BC03 and MILES line ratios. We calculate the misidentification fraction with the new sample and get a similar result: 21.5% of type II AGN identified by using BC03 templates are not identified as AGN when using MILES templates. Similarly, 28.1% of MILES type II AGN fall below the Kewley et al. (2001a) boundary when using MS11<sub>solar</sub> derived fluxes.

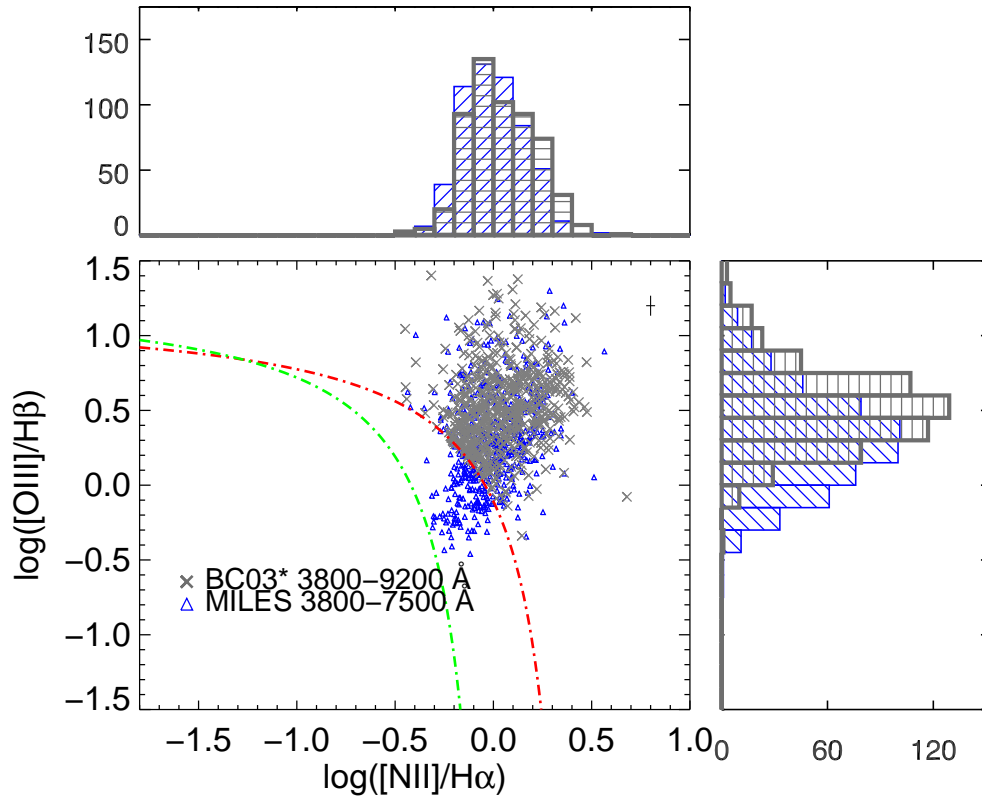


**Figure 8.** BC03-based line ratios (grey crosses) for 565 galaxies with  $S/N \geq 3$  above Kewley et al. (2001a) boundary. MILES-based ratios (blue triangles) for the same galaxies systematically shift downwards.

#### 4.1.1. Misidentification of LINERs and Seyfert II

Low-ionization narrow emission-line regions (LINERs) were first defined by Heckman (1980), and are different from Seyfert II galaxies. Typical LINERs have spectra features dominated by lines arising from low ionization states; their luminosities are similar to giant HII regions; and they are common. AGN located above the Kewley et al. (2001a) boundary in the  $[O\ III]/H\beta$ – $[N\ II]/H\alpha$  diagram can be either LINERs or Seyfert II. It is, therefore, pertinent to investigate if LINERs or Seyfert II dominates the misidentification rate. In addition,  $H\alpha$  equivalent width (EW)  $< 3\text{\AA}$  is proposed to be an indicator of LINERs whose emissions are from hot evolved stars (Cid Fernandes et al. 2010). The detailed discussion is in Appendix A. In summary, no significant difference is found in the misidentification rate between LINERs and Seyfert II. Since none of the misidentified Seyfert II or LINERs have  $H\alpha$  EW  $\leq 3\text{\AA}$ , it is unlikely the misidentified LINERs in our sample are powered by hot evolved stars.

#### 4.1.2. Dependence on data quality

Our study of the misidentified fraction as a function of the overall quality of the spectrum, i.e., the continuum  $S/N$  ratio is detailed in Appendix B. In summary, no strong correlation between the misidentified fraction and data quality is found.

#### 4.2. Comparisons of Templates

Fig 9 illustrates the difference in the best fit using the MILES and BC03 stellar population models as templates, zooming in on the best-fit ratios around the line regions we use to identify type II AGN candidates. The best fit using the MILES model predicts stronger Balmer lines (i.e.,  $H\alpha$  and  $H\beta$  lines) than that using BC03 templates. We show the flux variations between the results from BC03 and MILES template subtraction in Fig 10. The type II AGN identified by MILES template subtraction are highlighted in red circles. The mean flux of  $H\beta$  from BC03 type II AGN is  $\sim 26\%$  fainter than that from MILES templates, and the  $H\alpha$  line fit from BC03 is  $\sim 6\%$  fainter. Most of the type II

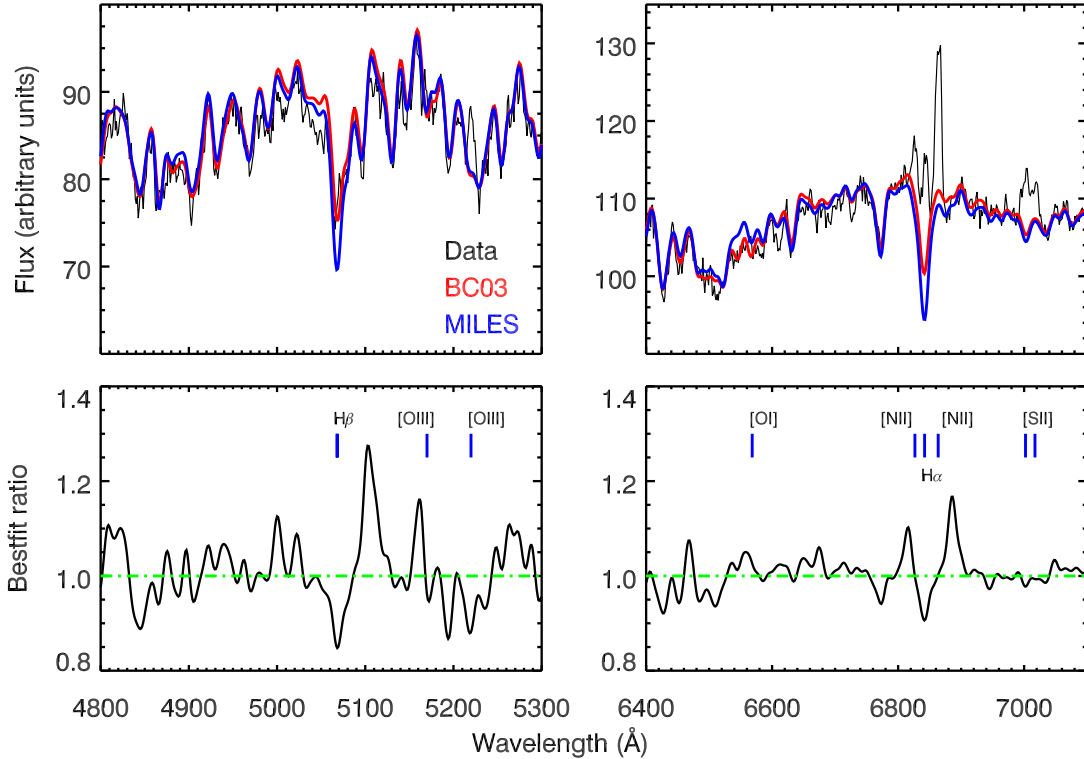


**Figure 9.** An example showing comparison of the best fit models from the full-spectrum-fitting result using MILES and BC03 as templates. The ‘bestfit ratio’ is the ratio between best fit derived by BC03 templates and the one derived by MILES templates.

AGN have stronger [O III] fluxes from BC03 than from MILES templates. The fluxes of [N II] from BC03 and MILES templates are consistent with each other. The inaccurate absorption lines of BC03 model is also described in detail by other groups (e.g., González Delgado et al. 2005; Koleva et al. 2008).

The differences between MILES and MS11<sub>solar</sub> are more surprising since they use the same input stellar library. This difference could be due to the treatment of the TP-AGB stars affecting SSPs between 0.2 to 2 Gyr. However, we examined the stellar population components of the sample galaxies, and found only 8% of them contain younger (age  $\leq 2$  Gyr) populations. In each of these galaxies, young stellar populations contribute less than 56% of the optical light. This means the systematic shift of line ratios when using MS11<sub>solar</sub> is not dominated by the special treatment of TP-AGB stars.

Furthermore, we note that we used all the available metallicities in the MILES model, and our best fits indicate that most ( $\sim 70\%$ ) of our galaxies favour metal-rich models, as shown in Fig 11. The green subsample highlights galaxies containing only one stellar population. While it is true that there is a degeneracy between age and metallicity when fitting only colors, as noted by Thomas et al. (2013), the degeneracy is lifted when simultaneously fitting both the absorption lines and the continuum (e.g., Reicherdt, Jimenez & Heavens 2001). Therefore, the choice of metallicity range of the templates also plays a role in type II AGN identifications. A detailed comparison between the stellar population models by Maraston and Strömbäck (2011) and Vazdekis et al. (2010) is beyond the scope of this work, and will not be addressed here.

#### 4.3. Young stellar populations and wavelength range

Young stellar populations ( $\leq 63$  Myr) are absent in all of the templates families discussed above. However, as we show in the Appendix C, the lack of young stellar populations does not significantly affect AGN identifications. We use G05 to explore young populations since empirical young SPMs are not available, and discuss the consistency between the G05 model and the MILES model at 63 Myr. An expansion of MILES model with G05 young population models is presented and used for AGN identification around the Kewley et al. (2001a) border. We also examined differences

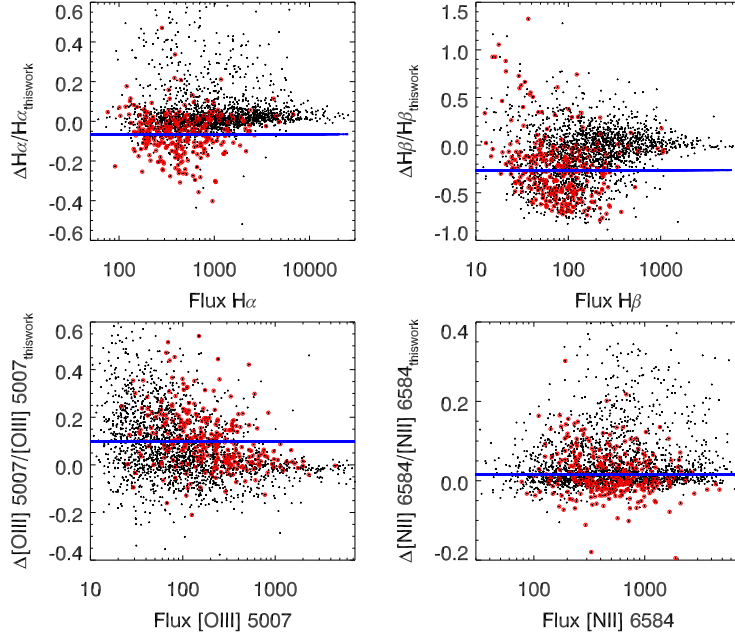


**Figure 10.** The difference of line fluxes between BC03 and this work (using MILES). This work, BC03, and MS11<sub>solar</sub> of the 2300 objects with  $S/N \geq 3$  of all four lines from both templates are shown in black crosses. Type II AGN (i.e., galaxies with line ratios above Kewley et al. (2001a) boundary in  $[O\ III]/H\beta - [N\ II]/H\alpha$  diagram) based on MILES template subtraction are shown as red circles. Note the line ratio scatters are large. We mark mean values of the line ratios of the type II AGN as blue lines in each panel.

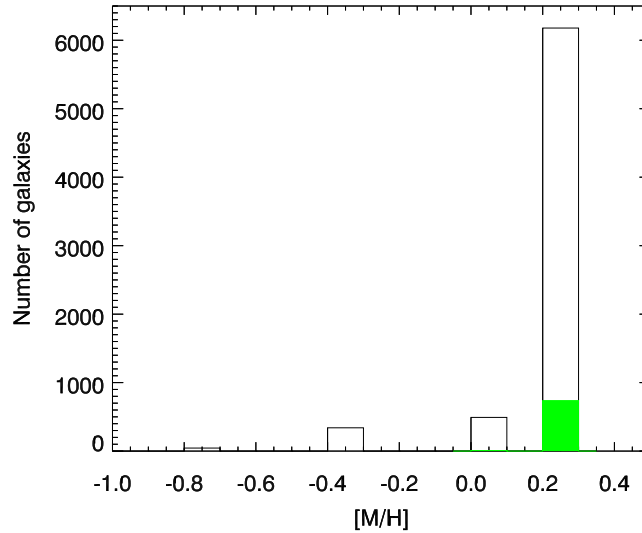


**Figure 11.** The metallicity distribution of the major population components of SDSS DR8 galaxies from the full-spectrum-fitting result. The green histogram shows the ones that contain only one simple stellar population.

due to wavelength ranges used in host galaxy subtraction in Appendix D. We find that young stellar populations (i.e. age  $\leq 63$ Myr) and the wavelength ranges used in the fit make little to no difference in AGN identification rates.

## 5. CONCLUSIONS

We have examined the differences in optical identification of type II AGN in nearby ( $z \leq 0.09$ ) galaxies with SDSS DR8 spectra, resulting from host galaxy subtraction using MILES, BC03, and MS11<sub>solar</sub> as stellar templates. We found that type II AGN identification is sensitive to the stellar template. Comparing the results of using the BC03 and MILES SPMs to subtract absorption lines in SDSS DR8 data, we determined that one quarter of the sample is misidentified as type II AGN by BC03 relative to MILES. Results using the MS11<sub>solar</sub> templates show fewer galaxies identified as AGN relative to MILES. We also find a 22% disagreement overall the work of Thomas et al. (2013), which used MS11<sub>solar</sub> for their host galaxy continuum and absorption subtraction. We traced the problem to the incomplete range of metallicities of the SPMs used in template fitting. The misidentification of both using BC03 (e.g., the work of MPA-JHU, SDSS DR8) and using MS11<sub>solar</sub> (e.g., the work of Thomas et al. (2013)) is greatest for objects with low [O III] luminosities, and is up to 50% for [O III] $\lambda$ 5007 luminosity fainter than  $10^{38}$  erg  $s^{-1}$ . The stellar population models used for the subtraction of the host galaxy contribution should be taken into account when using the emission line fluxes, or the AGN fractions, from a catalog especially if the results from different catalogs are compared.

#### ACKNOWLEDGMENTS

We thank YuXiao Dai who helped us in checking the data and some useful discussions. We thank Jong-Hak Woo for the discussion about AGN luminosities and AGN identifications. We thank the referee for his/her valuable comments and suggestions. The research of GRF was supported by National Science Foundation grants NSF-PHY-1212538 and NSF-AST-1517319, and by the James Simons Foundation.

Funding for SDSS-III has been provided by the Alfred P. Sloan Foundation, the Participating Institutions, the National Science Foundation, and the U.S. Department of Energy Office of Science. The SDSS-III web site is <http://www.sdss3.org/>.

SDSS-III is managed by the Astrophysical Research Consortium for the Participating Institutions of the SDSS-III Collaboration including the University of Arizona, the Brazilian Participation Group, Brookhaven National Laboratory, Carnegie Mellon University, University of Florida, the French Participation Group, the German Participation Group, Harvard University, the Instituto de Astrofísica de Canarias, the Michigan State/Notre Dame/JINA Participation Group, Johns Hopkins University, Lawrence Berkeley National Laboratory, Max Planck Institute for Astrophysics, Max Planck Institute for Extraterrestrial Physics, New Mexico State University, New York University, Ohio State University, Pennsylvania State University, University of Portsmouth, Princeton University, the Spanish Participation Group, University of Tokyo, University of Utah, Vanderbilt University, University of Virginia, University of Washington, and Yale University.

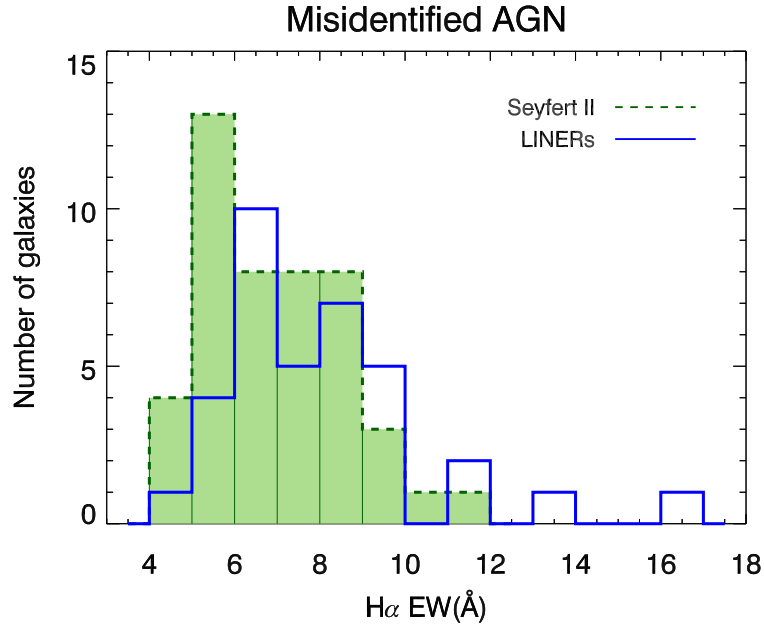


**Figure 12.**  $H\alpha$  EW distribution of misidentified Seyfert II and LINERs when using BC03 templates. The clear histogram shows distribution of the misidentified LINERs and the filled green histogram shows the  $H\alpha$  EW distribution of the misidentified Seyfert II.

## APPENDIX

### A. MISIDENTIFICATION OF LINERS AND SEYFERT II

Whether low-ionization nuclear emission-line regions (LINERs) are AGN is a topic that has been debated in literature. Ho (1996, 2008) and Masegosa et al. (2011), for example, argued that a significant fraction of LINERs are low-luminosity AGN. Other studies have suggested that LINERs are, instead, shock heated gas (Dopita & Sutherland 1995), starburst activity (Terlevich & Melnick 1985; Alonso-Herrero et al 2000), or post-AGB stars (Singh et al. 2013). Cid Fernandes et al. (2010) suggest that  $H\alpha$  EW can differentiate between the different ionization mechanisms which lead to the overlap in the LINER region of traditional diagnostic diagrams. According to the bimodal distribution of  $H\alpha$  EW, Cid Fernandes et al. (2011) suggest that LINERs with  $H\alpha$  EW  $> 3 \text{ \AA}$  are likely to be true AGN, while those with  $H\alpha$  EW  $< 3 \text{ \AA}$  have emissions from hot evolved stars.

In order to discern the nature of the LINERs in our sample using the  $H\alpha$  EW, we first separate the AGN identified from MILES based line ratios into LINERs and Seyfert II using the Kewley et al. (2006) criteria. Fig 12 shows the misidentified LINERs and Seyfert II when using BC03 templates as a function of  $H\alpha$  EW. None of the galaxies are found to have  $H\alpha$  EW  $< 3 \text{ \AA}$ . Therefore, there are no LINERs powered by hot evolved stars, as defined by Cid Fernandes et al. (2010), in our misidentified sample. The misidentification instead mainly comes from line ratio variations due to template subtraction. Furthermore, Fig 12 shows that no clear separation of  $H\alpha$  EW distribution is observed between the misidentified LINERs and Seyfert II galaxies.

The line ratios based on MILES template-subtraction is shown in Fig 13 panel (a). Galaxies are limited to the sample with  $S/N \geq 3$  for all four lines in all three templates. Seyfert II are shown in purple and LINERs are shown in dark green. We also show the line ratios based on BC03 in panel (b) and line ratios based on MS11<sub>solar</sub> in panel (c) for the same galaxies. As clearly shown in the plots, line ratios derived from the different template-subtractions show systematic shifts. BC03 based line ratios shift towards the AGN/Seyfert II regions; while the MS11<sub>solar</sub> based line ratios show the opposite trend.

Of the Seyfert II identified using BC03, 20.7% fall below the Kewley et al. (2001a) using MILES-based line ratios. Similarly, the false positive rate of the BC03 LINERs is 14.6%. Our investigation of MS11<sub>solar</sub> based line ratios shows

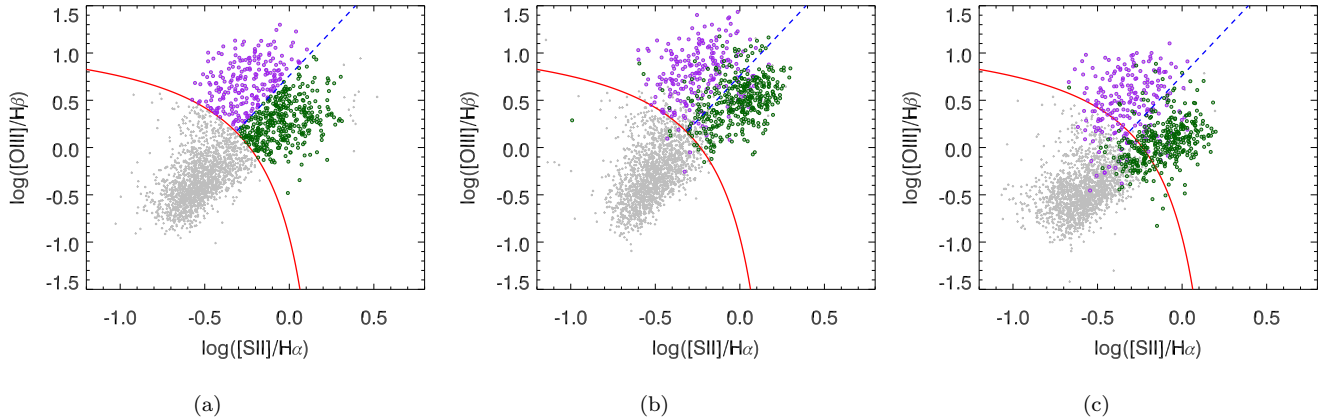


**Figure 13.** Panel (a): Line ratios based on MILES template-subtraction to show the distribution of star-forming galaxies, Seyferts, and LINERS.  $S/N \geq 3$  were set up for all four lines from all three templates. The Kewley et al. (2006) boundary (the blue dashed line) is adopted to distinguish Seyferts and LINERS, where Seyferts are shown as purple circles, and LINERS are shown as green circles. Panel (b): Line ratios based on BC03 for the same galaxies in panel (a). Panel (c): Line ratios based on MS11<sub>solar</sub> for the same galaxies in panel (a). The colors for panels (b) and (c) are based on MILES classifications.

a 26.0% false negative rate for Seyfert II and a 27.7% false negative rate for LINERS. Roughly half of the misidentified galaxies are (were) Seyfert II and half are (were) LINERS.

## B. DEPENDENCE ON DATA QUALITY

We examine the misidentified AGN fraction against the overall data quality of the spectrum, i.e., the continuum  $S/N$  ratio. Since  $S/N$  varies at different wavelengths, we choose the continuum  $S/N$  near the  $H\beta$  line (hereafter  $S/N(H\beta)$ ) for this purpose as  $H\beta$  is the weakest of the four type II AGN identification lines. Figure 14a shows the distribution of  $S/N(H\beta)$  for type II AGN. The green histogram highlights the type II AGN identified when using BC03 templates, but not as type II AGN, when using MILES templates. The misidentification rate shows a weak dependence of  $S/N(H\beta)$  as seen in Fig 14b. Exploration of the dependence between [O III]5007 luminosity and  $S/N(H\beta)$  is shown in Fig 14c. Misidentified type II AGN are shown as filled red triangles. No strong correlation is found.

We show the result from MS11<sub>solar</sub> templates in Figure 15. The distribution of  $S/N(H\beta)$  for type II AGN identified from MILES templates, but not from MS11<sub>solar</sub> templates, are shown in the green histogram. Misidentification rate as a function of  $S/N(H\beta)$  is shown in Fig 15b. The result is similar to the comparison between MILES and BC03, except for the first  $S/N$  bin that contains low statistics. We also explore the dependence between [O III]5007 luminosity and  $S/N(H\beta)$ . As shown in Fig 15c, misidentified type II AGN are shown as filled red triangles. No strong correlation is found. The misidentification of type II AGN is, therefore, not due to data quality.

## C. EFFECTS OF YOUNG STELLAR POPULATIONS

### C.1. Young stellar populations

Comparing parameters of the BC03 and MILES models in Table 1, we note that BC03 contains younger stellar populations than MILES. Young stellar populations are hard to model due to the lack of empirical observations. BC03 models have young stellar populations with a corrected continuum but their lines have not been corrected (Bruzual & Charlot 2003, Section 2.2.3), especially at non-solar metallicities (González Delgado et al. 2005). We instead resort to theoretical young stellar populations. We expand the MILES model by adding young theoretical stellar population templates from G05 to make up for the fact that there are not many empirical stellar libraries covering that parameter space. As pointed out by Charlot & Fall (2000), stellar populations younger than  $\sim 3$ -4 Myr do not contribute to the observed spectra, because their absorption features are hidden behind their optically thick HII cloud. We therefore have confidence that using the models by González Delgado et al. (2005) at a youngest age of 4 Myr is adequate. To check the consistency between the G05 theoretical model and MILES model, we compare the spectra of their populations at the common age of 63 Myr, the youngest stellar population in the MILES model, at metallicities of  $[Fe/H] = -0.4$  and  $[Fe/H] = 0.0$  (solar metallicity). As shown in Fig 16, the G05 and MILES

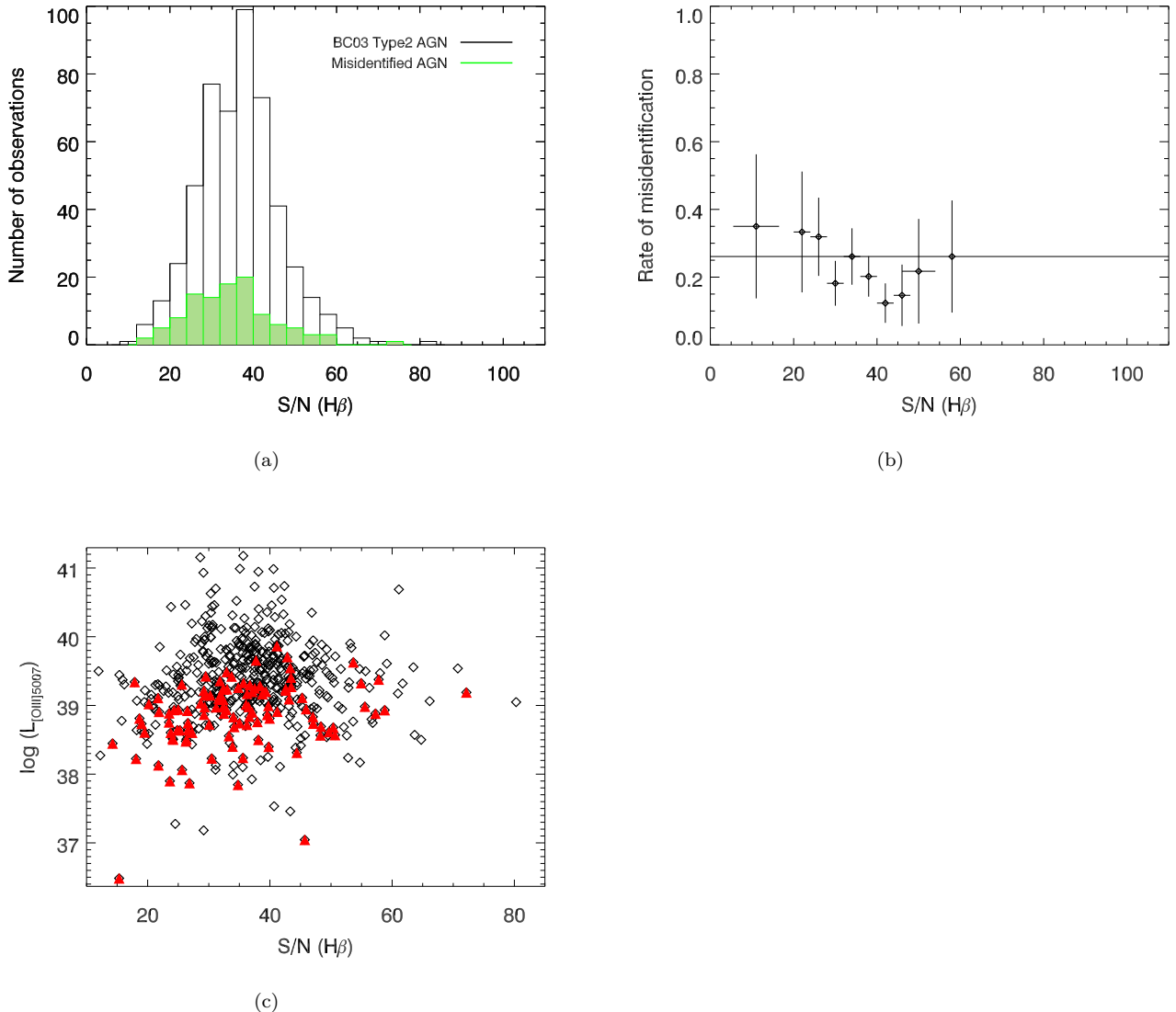


**Figure 14.** BC03 based misidentification as a function of data quality near H $\beta$  line. Panel (a): the clear histogram shows all type II AGN identified by using BC03 templates. The misidentified type II AGN are shown in filled green histogram. Panel (b): The misidentification rate as a function of continuum S/N near H $\beta$  line. Panel (c): The luminosity of [O III] $\lambda$ 5007 of type II AGN from BC03 template subtraction as a function of continuum S/N near H $\beta$  line are shown as black diamonds. The misidentified type II AGN are marked by filled red triangles.

models are in general consistent with each other even at the boundary of the MILES model, with less than 10 percent deviation in their residual spectra.

### C.2. AGN identification with the addition of young stellar populations

The consistency discussed above gives us confidence that mixing theoretical and empirical models does not introduce systematic effects. Because the wavelength range in González Delgado et al. (2005) is slightly shorter than MILES, we truncate the MILES model to the common wavelength range  $\lambda\lambda 3500 - 7000 \text{ \AA}$ . All stellar population models younger than 63 Myr from González Delgado et al. (2005) were broadened to the same resolution as MILES.

Following our initial strategy, we limit the sample within 0.02 dex around the Kewley et al. (2001a) boundary in BPT diagram to investigate the line ratio variations. We fit the SDSS spectra using the young-population-extended MILES templates. We found that only three objects out of the 145 boundary galaxies contain young population components, with a contribution less than four percent in each of the cases. Fits for the other 142 galaxies give almost exactly the



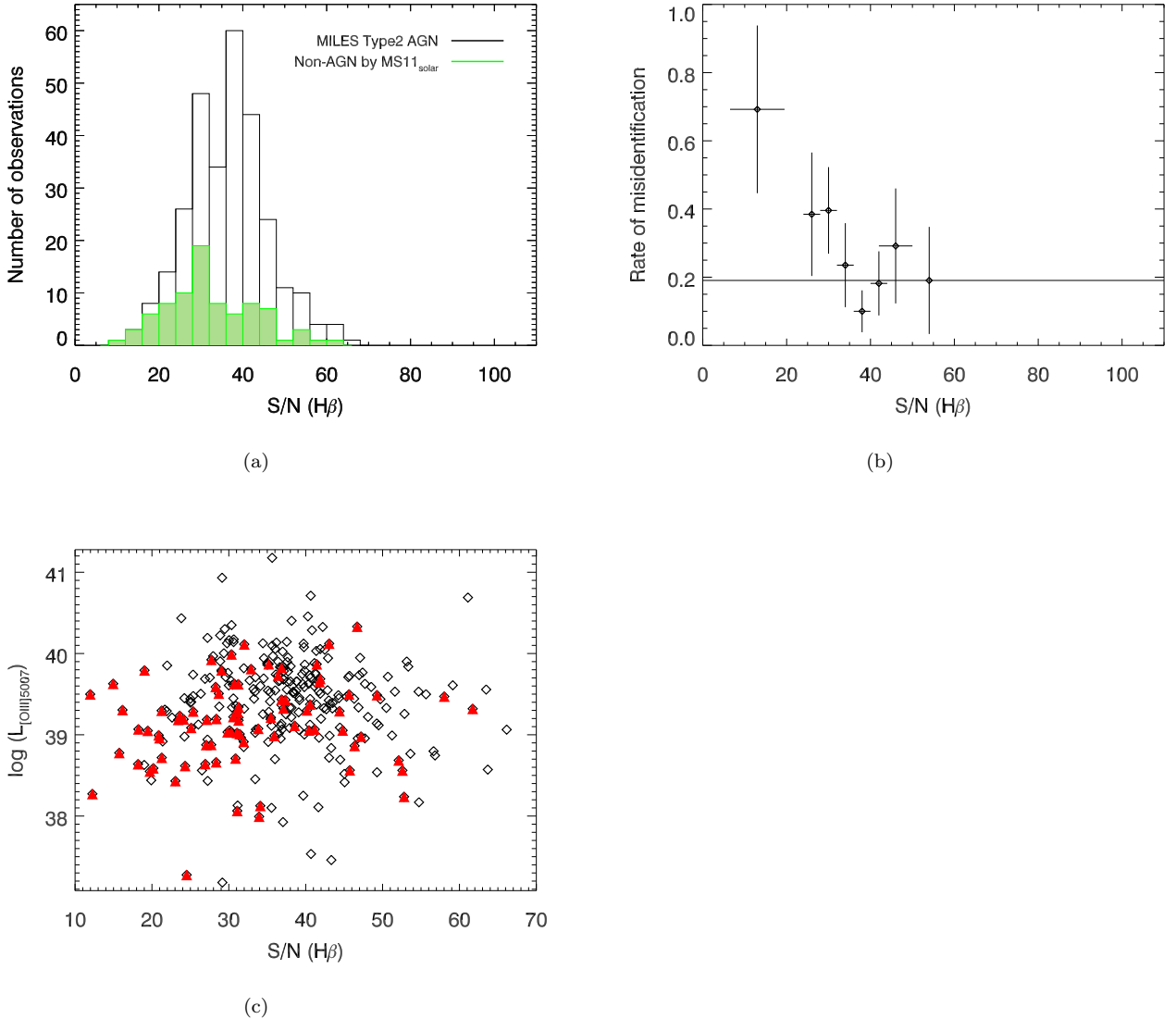


**Figure 15.** MS11<sub>solar</sub> based misidentification as a function of data quality near H $\beta$  line. Panel (a): the clear histogram shows all type II AGN identified by using MS11<sub>solar</sub> templates. The misidentified type II AGN are shown in filled green histogram. Panel (b): The misidentification rate as a function of continuum S/N near H $\beta$  line. Panel (c): The luminosity of [O III]5007 of type II AGN from MS11<sub>solar</sub> template subtraction as a function of continuum S/N near H $\beta$  line are shown as black diamonds. The misidentified type II AGN are marked by filled red triangles.

same result as using only MILES templates in the same wavelength coverage, as shown in Fig 17. In fact, even those three objects show only small shifts in the line ratios,  $\sim 0.03$  in [O III]/H $\beta$  and  $\sim 0.002$  in [N II]/H $\alpha$ , far smaller than the typical line ratio errors. As shown by the olive diamonds (MILES + G05 young populations) overlapped with the red dots (MILES only, wavelength truncated to the same range as MILES + G05), there are no significant changes resulting from adding younger templates.

#### D. WAVELENGTH RANGE DEPENDENCE

We also considered whether the wavelength range used for the spectrum fitting and absorption and continuum component subtraction may play a role in AGN identification. We performed this test using both the BC03 templates and MILES templates.

As mentioned above, we expanded the MILES models with young stellar populations with G05 with truncated wavelength 3500–7000 Å since the red wavelength limit of G05 models is 7000 Å. The line ratio variation from wavelength

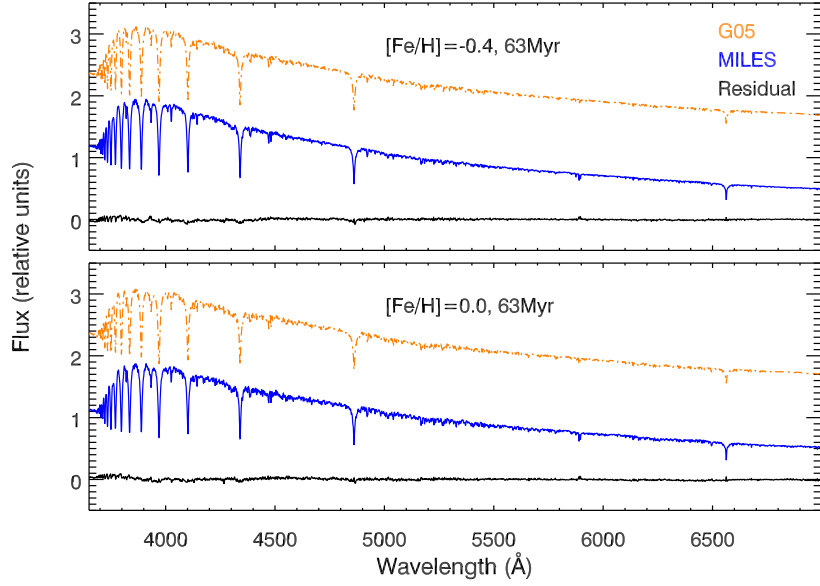


**Figure 16.** G05 templates of 63 Myr at two metallicities compared with the MILES model. G05 templates were smoothed to the same resolution as MILES library of  $\text{FWHM}=2.5 \text{ \AA}$ . The residual spectra are the difference between these two sets of models.

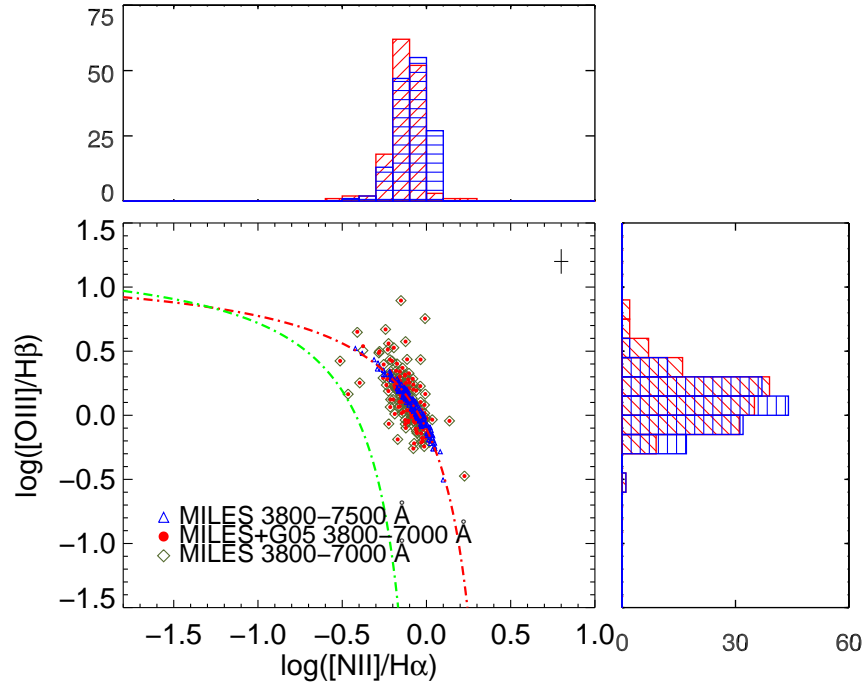


**Figure 17.** The same galaxies based on MILES template subtraction within 0.02 dex around the Kewley et al. (2001a) boundary selected as in Fig 5, with addition of the line ratios derived from young-stellar- population-extended MILES templates (red dots) and wavelength-truncated MILES templates (olive diamonds). Agreement of red dots and olive diamonds shows that adding young stellar population templates does not change the line ratios. The line ratios derived from truncated templates cause a larger scatter around the Kewley et al. (2001a) boundary. The distributions of line ratios are histogrammed on the side of the axes. The colors of histograms are the same as for the BPT diagram.

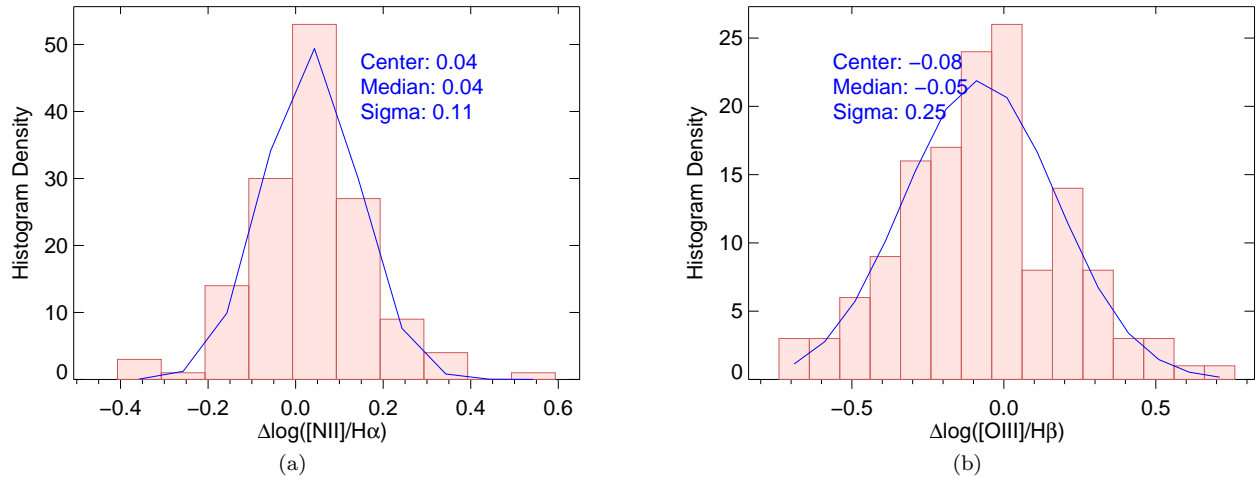


**Figure 18.** Distribution of line ratio differences between the fits with MILES model in wavelength range of 3800–7500Å and 3800–7000Å. Left panel shows the difference in the [N II]/H $\alpha$  ratio; right panel shows that difference in the [O III]/H $\beta$  ratio.

truncation of MILES templates is shown in Fig 17. Compared to the line ratios derived from the full wavelength range of MILES,  $\lambda\lambda 3800 - 7500\text{\AA}$ , the result with truncated MILES templates shows scattered line ratios around the Kewley et al. (2001a) boundary but no strong systematic effects. Fig 17 illustrates the distribution of the line ratios: by truncating only 400–500 Å in the red, the line ratios scatter more around the Kewley et al. (2001a) boundary, sharing the similar ranges of [O III]/H $\beta$  and [N II]/H $\alpha$ . We compare the line ratio differences in Fig 18. It shows that the centre of [N II]/H $\alpha$  is shifted by 0.04 dex, and the centre of [O III]/H $\beta$  is shifted by -0.05 dex. The line ratio offsets of both [N II]/H $\alpha$  and [O III]/H $\beta$  are consistent with zero within the errors.

We changed the fitting wavelength range to be  $\lambda\lambda 3800 - 7500\text{\AA}$  in testing the BC03 templates. The results are shown in Fig 19 to illustrate the difference from the original fitting wavelength of  $\lambda\lambda 3800 - 9200\text{\AA}$ . The grey histograms show the distribution of SDSS DR8 line ratios, and the golden histograms show the line ratios derived by truncated spectrum-fitting using BC03. The line ratios from truncated wavelength fit, still scatter around the same region in the BPT diagram as the result from wider wavelength range.

A detailed systematic analysis on the line ratios of truncated BC03 templates is shown in Fig 20. A shift of 0.08 dex is observed in [O III]/H $\beta$ , and a shift of  $\sim 0.01$  dex is observed in [N II]/H $\alpha$ . Again, the line ratio offsets of both [N II]/H $\alpha$  and [O III]/H $\beta$  are consistent with zero within the errors.

## REFERENCES

- Aihara, H., Allende Prieto, C., An, D., et al., 2011, ApJS, 195, 26A
- Allen, J. T., Hewett, P. C., Richardson, C. T., Ferland, G. J., Baldwin, J. A., 2013, MNRAS, 430, 3510A
- Alonso-Herrero, A., Rieke, M. J., Rieke, G. H., and Shields, J. C. 2000, ApJ, 530, 688
- Baldwin, J. A., Phillips, M. M., Terlevich, R. 1981, PASP, 93, 5B
- Bruzual, G. & Charlot, S. 2003, MNRAS, 344, 1000B
- Cappellari, M. & Emsellem, E. 2004 PASP, 116, 138
- Charlot, S. & Fall, S. M., 2000, ApJ, 539, 718C
- Chen, Yan-Ping, Trager, S. C., Peletier, R. F., et al. 2014, A&A, 565A,117C
- Cid Fernandes, R. and Stasińska, G. and Schlickmann, 2010, MNRAS, 403, 1036C
- Cid Fernandes, R., Stasińska, G., Mateus, A., Vale Asari, N., 2011, MNRAS, 413, 1687
- Conroy, Charlie & Gunn, James E. 2010, ApJ, 712, 833C
- Conroy, C. 2013, ARA&A, 51, 393C
- Dopita, M. A., & Sutherland, R. S. 1995, ApJ, 455, 468
- González Delgado, R. M., Cerviño, M., Martins, L. P., Leitherer, C., Hauschildt, P. H. 2005, MNRAS, 357, 945G
- Greene, J. E. & Ho, L. C. 2007, ApJ, 667, 131G
- Gregg, M. D., Silva, D., Rayner, J., et al. 2006, hstc, conf, 209G

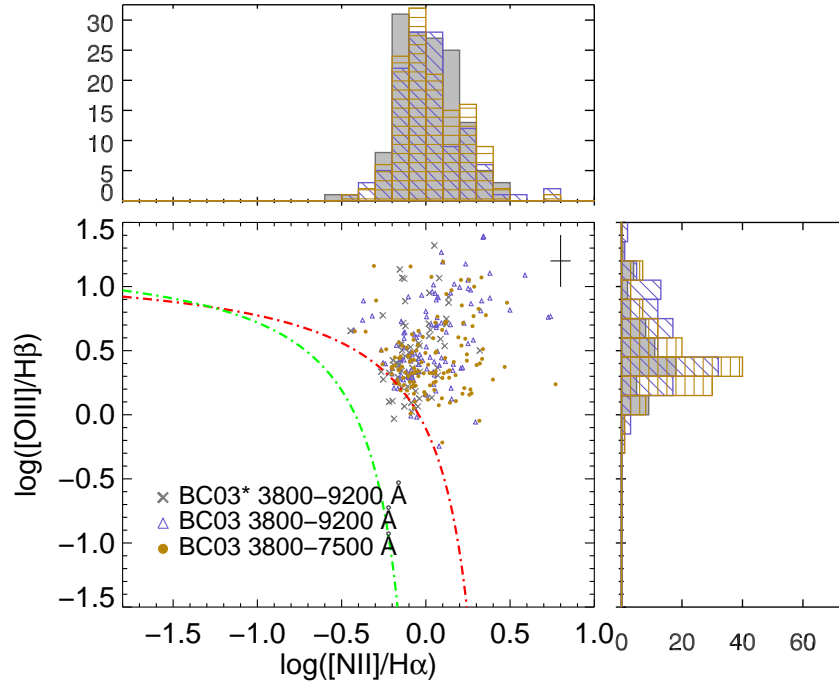


**Figure 19.** BC03-based line ratios for 145 objects near the [Kewley et al. \(2001a\)](#) boundary as defined in Fig 5. The grey crosses are directly from SDSS DR8 archive, the purple triangles are from this work, the golden dots are from the wavelength-truncated BC03 templates. The distributions of line ratios are histogrammed on the side of the axes. The colors are the same as the line ratios.

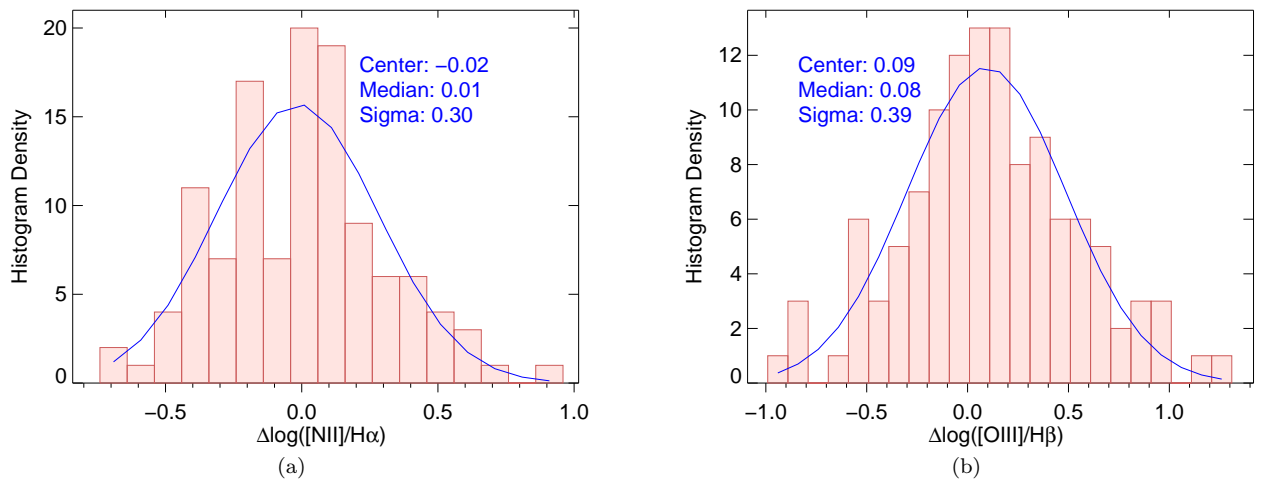


**Figure 20.** Distribution of line ratio differences between the fits with BC03 templates in wavelength range of 3800–9200Å and 3800–7400Å. Left panel shows the difference of line ratio  $[N II]/H\alpha$ ; right panel shows that difference of line ratio  $[O III]/H\beta$ .

- Hao, L., Strauss, M. A., Tremonti, C. A., et al. 2005, *AJ*, 129, 1783H
- Heckman, T. M., 1980, *A&A*, 87, 152H
- Ho, L. C., 1996, *ASPC*, 103, 103H
- Ho, L. C., Filippenko, A. V., Sargent, W. L. W. 1997, *ApJS*, 112, 315H
- Ho, L. C., 2008, *ARA&A*, 46, 475H
- Huchra, J. P., Macri, L. M., Masters, K. L., et al. 2012, *ApJS*, 199, 26
- Kauffmann, G., Heckman, T. M., Tremonti, C., et al. 2003, *MNRAS*, 346, 1055K
- Kewley, L. J., Heisler, C. A., Dopita, M. A., et al. 2000, *ApJ*, 530, 704K
- Kewley, L. J. and Dopita, M. A., Sutherland, R. S., Heisler, C. A., Trevena, J. 2001a, *ApJ*, 556, 121K
- Kewley, L. J., Heisler, C. A., Dopita, M. A., Lumsden, S. 2001b, *ApJS*, 132, 37K
- Kewley, L. J., Groves, B., Kauffmann, G., Heckman, T. 2006, *MNRAS*, 372, 961K
- Koleva, M., Prugniel, P., Ocvirk, P., Le Borgne, D., Soubiran, C., 2008, *MNRAS*, 385, 1998K
- Le Borgne, J.-F., Bruzual, G., Pelló, R., et al. 2003, *A&A*, 402, 433L
- Le Borgne, D., Rocca-Volmerange, B., Prugniel, P., et al. 2004, *A&A*, 425, 881L
- Lejeune, Th., Cuisinier, F., Buser, R. 1997, *A&AS*, 125, 229L
- Lejeune, Th., Cuisinier, F., Buser, R. 1998, *A&AS*, 130, 65L
- Maraston, C., Strömbäck, G. 2011, *MNRAS*, 418, 2785M
- Masegosa, J., Márquez, I., Ramirez, A., González-Martín, O., 2011, *A&A*, 527A, 23M
- Miller, C. J. and Nichol, R. C., Gómez, P. L., Hopkins, A. M., Bernardi, M. 2003, *ApJ*, 597, 142M
- Osterbrock, D., E., Pogge, R., W., 1985, *ApJ*, 297, 166O
- Prugniel, Ph., Soubiran, C. 2001, *A&A*, 369, 1048P
- Reichardt, C., Jimenez, R., Heavens, A. F., 2001, *MNRAS*, 327, 849R
- Sánchez-Blázquez, P., Peletier, R. F., Jiménez-Vicente, J., et al. 2006, *MNRAS*, 371, 703S
- Singh, R., van de Ven, G., Jahnke, K., et al., 2013, *A&A*, 558A, 43S
- Stasińska, G., Cid Fernandes, R., Mateus, A., Sodré, L., Asari, N. V., 2006, *MNRAS*, 371, 972S
- Terlevich, R., & Melnick, J. 1985, *MNRAS*, 213, 841
- Thomas, D., Steele, O., Maraston, C., et al. 2013, *MNRAS*, 431, 1383T
- Vazdekis, A., Sánchez-Blázquez, P., Falcón-Barroso, J., et al. 2010, *MNRAS*, 404, 1639V
- Vazdekis, A., Ricciardelli, E., Cenarro, A. J., et al. 2012, *MNRAS*, 424, 157V
- Vazdekis, A., Koleva, M., Ricciardelli, E., Röck, B., Falcón-Barroso, J. 2016, *MNRAS*, 463, 3409V
- Veilluex, S., Osterbrock, E., E., 1987, *ApJS*, 63, 295V
- Westera, P., Lejeune, T., Buser, R., Cuisinier, F., Bruzual, G. 2002, *A&A*, 381, 524W
- York, D. G., Adelman, J., Anderson, Jr., J. E., et al. 2000AJ, 120, 1579Y